# Supercritical fluid technology : a reliable process for high quality BaTiO3 based nanomaterials

Cyril Aymonier, Catherine Elissalde, Gilles Philippot, Mario Maglione

Advanced Powder Technology 25 (2014) 1415–1429

Contents lists available at ScienceDirect

Advanced Powder Technology

journal homepage: www.elsevier.com/locate/apt

Review paper

# Supercritical fluid technology: A reliable process for high quality $BaTiO_3$ based nanomaterials ☆

Gilles Philippot, Catherine Elissalde, Mario Maglione, Cyril Aymonier *

*CNRS, ICMCB, UPR 9048, F-33600 Pessac, France*
*Univ. Bordeaux, ICMCB, UPR 9048, F-33600 Pessac, France*

ARTICLE INFO

*Article history:*
Received 6 December 2013
Received in revised form 23 January 2014
Accepted 15 February 2014
Available online 1 March 2014

*Keywords:*
Supercritical fluids
Ferroelectric
Nanoparticle
Defects
Core–shell

ABSTRACT

Ferroelectrics materials have been tremendously attractive since the 40 s with the discovery of ferroelectricity in metal oxide perovskite materials and more precisely in barium titanate. Due to their high potential for industrial applications, intensive research has been carried out to better understand their behavior and develop processes to produce them. Trying to face the down scaling demand of high quality particles towards the nanometer range, some conventional methods such as the solid state one reach their limits. The development of other processes are thus required and the synthesis in supercritical fluids can be considered as a promising alternative. This technology exhibits very interesting characteristics such as fast continuous synthesis (few seconds) of high quality nanoparticles (well crystallized nanoparticles with narrow size distribution) with controlled composition ($Ba_{1-x}Sr_xTiO_3$ with $0 \leqslant x \leqslant 1$) at intermediate synthesis temperatures (<400 °C) with the use of non-toxic solvents (water, ethanol). Reaching the nanometer size range, the intrinsic properties of ferroelectric materials change compared to the bulk. Consequently a deep study concerning the crystalline structure, the presence of defects and the surface chemistry of those nanoparticles has to be achieved to control their properties for further use in functional devices.



**Contents**



☆ Open Access for this article was sponsored by the Society of Powder Technology, Japan, through the Grant-in-Aid for Publication of Scientific Research Results, Japan Society for the Promotion of Science, 2013.

* Corresponding author. Address: ICMCB-CNRS, 87 avenue du Dr. Albert Schweitzer, 33608 Pessac Cedex, France. Tel.: +33 540002672.
*E-mail address:* aymonier@icmcb-bordeaux.cnrs.fr (C. Aymonier).

http://dx.doi.org/10.1016/j.apt.2014.02.016
0921-8831/

## 1. Introduction

The history of ferroelectricity starts in the 17th century when Elie Seignette synthesized a salt of sodium potassium tartrate tetrahydrate (or Rochelle salt) for medical applications. It is only several decades later that other interesting properties were discovered like the piezoelectricity in 1880 [1], the pyroelectricity in 1824 [2] and finally the ferroelectricity in the early 1900s [3–5]. The Second World War will be at the origin of a major progress with the discovery of ferroelectricity in perovskite based ceramics. Among the different ceramics studied, barium titanate ($BaTiO_3$ or BT) appeared as one of the most promising candidate with a dielectric permittivity ($\varepsilon_r > 1000$ at room temperature) much higher than for others ceramics such as $TiO_2$ and $CaTiO_3$ ($\varepsilon_r < 100$ at room temperature) [6–10].

The high potential of these materials in terms of industrial applications dragged intensive researches in order to better understand and improve their properties. Nowadays such materials find a tremendous amount of applications which can go from specific high technology to basic everyday life devices. They are used in computers (ferroelectric memories), security systems (pyroelectric sensors), optical communication devices (electro-optic films), micro speakers (piezoelectric transducers), as passive components in microelectronic circuits (capacitors) and so on [11].

Industry, which always pushes away boundaries in terms of devices size, performance, functionalities and reliability, expects more and more the use of low cost high quality nanopowders. The continuous advances in microelectronics and communications lead to the miniaturization of ferroelectric components. As an illustration multi-layer ceramic capacitors (MLCC) have undergone a remarkable size reduction for 30 years. To be able to achieve high capacitance in a small volume (increase of the volumetric efficiency), the dielectric layer thickness has to be reduced while increasing the number of layers. The dielectric thickness ranges from 2.0 to 0.8 μm and the grain size within each layer should become less than 100 nm [12–17]. However, this size decrease has a direct impact on the dielectric properties of the material. That is why it is critical to produce well crystallized particles with a narrow size distribution in order to control the permittivity and reduce the creation of defects during the processing and integration of these powders into electronic devices [18].

Currently there are three main synthesis processes to produce such materials: the solid state route, the sol–gel method and the hydrothermal process. Nevertheless, in the context of such size down scaling, these conventional synthesis routes reach their limits in terms of material characteristics but also production costs or time, triggering the development of alternative processes. A promising approach is the synthesis of ferroelectric nanopowders using supercritical fluids; this scalable technology enables a single step synthesis of high quality nanoparticles at moderate temperatures (<400 °C) and in tens of seconds.

This literature review presents a summary of the supercritical fluid technology interests towards nanomaterials synthesis with a focus on the ferroelectric metal oxides. First a background concerning the ferroelectricity origin is presented using the example of $BaTiO_3$. It is followed by a description of the most well-known synthesis routes and their limitations in terms of expected materials characteristics (size, size distribution, composition, homogeneity, etc.) and cost. Finally the supercritical fluid technology principle, interests and field of applications are introduced and illustrated with the example of $BaTiO_3$ synthesis, characterization and performances.

## 2. Origin of ferroelectricity

### 2.1. Background

Crystal structures can be divided into 32 classes, or point groups, according to the number of rotational axes and mirror planes they exhibit (Fig. 1). Amoung the thirty-two crystal classes, twenty-one are non-centrosymmetric and of these, twenty exhibit piezoelectricity. Only 10 of the 32 point groups are polar, having a dipole in their unit cell, and exhibiting pyroelectricity. Finally, inside those ten classes few of them are going to present the ferroelectric property which is the ability of tuning the material's polarization according to different stable directions applying an electric field [7,19].

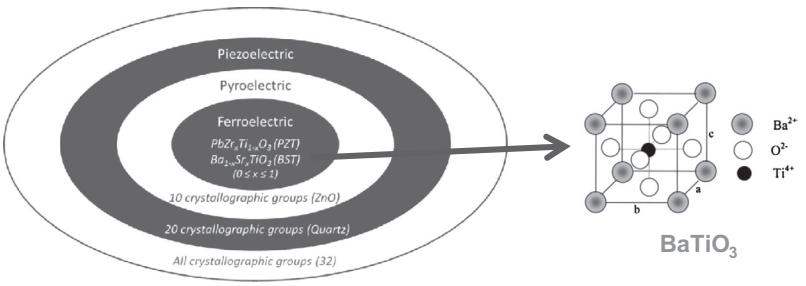


**Fig. 1.** Classification of the various properties based on their crystal structure with the example of the paraelectric cubic perovskite structure of $BaTiO_3$ 'Adapted from ref. [21]'.

As illustrated in Fig. 2, once the material is poled, switching the orientation of the domains within the material induces a hysteresis loop. The remanent polarization ($P_r$) corresponds to the material's polarization without an applied electric field ($E$) and the saturation polarization ($P_S$) is reached in the high field range. Finally, the coercive field ($E_{Coerc.}$) is the switching field [20].

### 2.2. Perovskite structure

The unit cell of the perovskite structure ($ABO_3$) is presented in Fig. 1 through the example of $BaTiO_3$ where the titanium atom occupies the B site within the oxygens octahedron, the barium atoms are at the corners and the oxygen atoms at the center of the faces. The temperature at which the spontaneous polarization disappears is called the Curie temperature, $T_{Curie}$. Above 120 °C, the barium titanate has a cubic structure exhibiting a centro-symmetry with no spontaneous dipole. Below 120 °C, it turns into a tetragonal phase, with a displacement of the Ti atoms inside the $O_6$ octahedra [21].

### 2.3. Phase transitions and dielectric permittivity

Fig. 3 shows an overview of the $BaTiO_3$ dielectric permittivity variations as a function of the temperature. At high temperature $BaTiO_3$ has a paraelectric cubic perovskite phase. As the temperature decreases, it undergoes three successive transitions to ferroelectric phases with tetragonal, orthorhombic and rhombohedral symmetries at respectively 120, 0 and −90 °C. The maximum of permittivity occurs at $T_{Curie}$ [22].

Substituting some barium atoms with strontium ones, $T_{Curie}$ can be tuned across room temperature (Fig. 4) enabling an adjustment

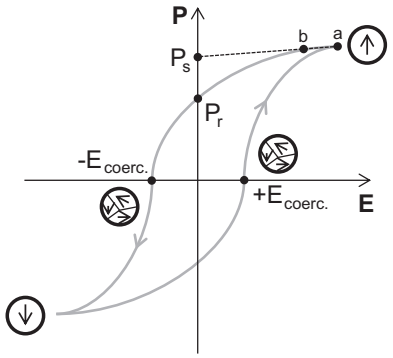


**Fig. 2.** Ferroelectric hysteresis loop with the representation of the polarization state in the circles.

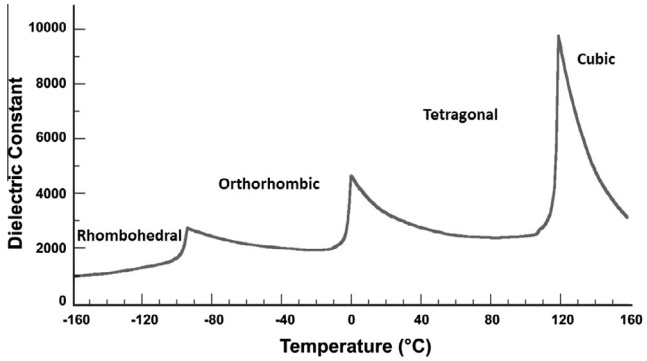


**Fig. 3.** Evolution of $BaTiO_3$ dielectric permittivity according to the temperature 'Adapted from ref. [22]'.

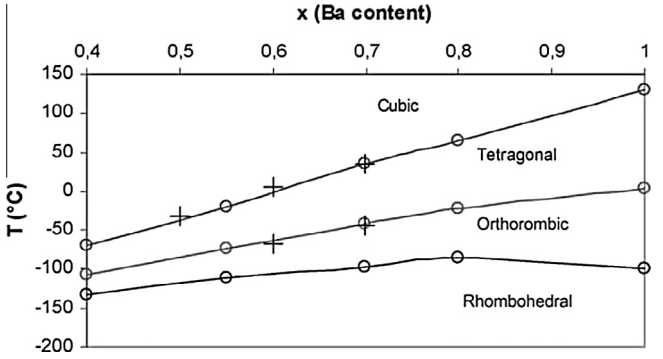


**Fig. 4.** Effect of barium substitution with strontium on phase transition temperatures 'Reprinted from ref. [23] Copyright © (2005), Elsevier'.

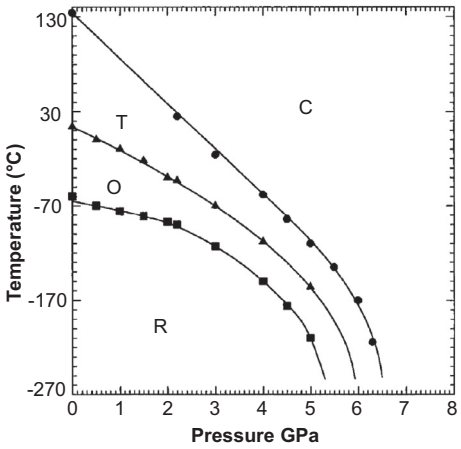


**Fig. 5.** $BaTiO_3$ pressure–temperature phase diagram 'Reprinted from ref. [24] Copyright © (1997), American Physical Society'.

of the permittivity [23]. Ishidate et al. [24] experimentally demonstrated that applying an external pressure on the material will have a similar effect as the strontium substitution. As presented in Fig. 5, according to the applied force direction on the material, the geometry of the cell will be modified from a tetragonal to a cubic phase at a given temperature. For example, with a pressure of 2.3 GPa they observed a phase transition from the tetragonal to the cubic one at room temperature. The lattice contraction was estimated at 0.023 Å comparable to the case of barium substitution with strontium. Indeed, with 30% of barium replaced with strontium the same phase transition will also occur at room temperature with an associated lattice contraction of 0.03 Å. Those two values being close they conclude that the strontium substitution and the pressure applied play an equivalent role concerning the phase transition temperature variations.

### 2.4. Size effect

The properties of ferroelectric materials are intimately related to the crystal structure and chemical composition. Moreover the permittivity of $BaTiO_3$ ceramics also strongly depends on the grain size. Fig. 6 reports several literature works regarding the grain size dependence on permittivity underlining the values spreading and the strong influence of both the synthesis and sintering methods [25].

In addition the Curie temperature decreases with the grain size, and below 100 nm the structure is no more tetragonal at room temperature [26,27]. Such size effect has been explained by

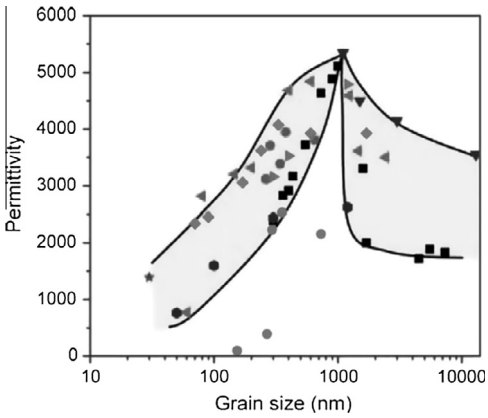


**Fig. 6.** $BaTiO_3$ dielectric permittivity ($\varepsilon$) as a function of grain size' Reprinted from ref. [25] Copyright © (2011), Elsevier'.

different models: (1) the internal stress model based on the change in domain structure [28–30], (2) the surface stress model based on the existence of a "dead layer" at the surface of the particles [13,31,32] and (3) the nanoparticles composite structure consisting of an inner tetragonal core, a gradient lattice strain layer (GLSL), and a surface cubic layer [33,34]. Those different models and their consequences on the ferroelectric properties will be developed in the discussion section of this paper. Being focused on powder processing, the ferroelectricity in nanocrystals etched from bulk crystals will not be addressed here [35].

In this first introductive part the ferroelectricity dependences on the material's crystalline structure were shown. In addition the intrinsic properties sensitivity to the size downscaling towards the nanometer range was highlighted. It is thus important to develop synthesis methods enabling a high level of control on the material characteristics (size, size distribution, composition, purity, etc.) from the early stage of its processing. In the following part a state of the art concerning the main synthesis routes is presented and illustrated through the example of $BaTiO_3$ synthesis.

## 3. $BaTiO_3$ main synthesis routes

The challenge is to have a process enabling the large scale synthesis of the material fulfilling the expectations in terms of characteristics while keeping in mind the economic and environmental requirements. Table 1 summarizes the most well-known synthesis routes reported in the literature to produce metal oxide materials. They can be divided in three categories: (1) the dry processes with deposition (chemical vapor deposition, atomic layer deposition or physical vapor deposition) [36–42], molten salts [43–48] and solid state [7,21,49–54] methods, (2) the wet processes with sol–gel [55–58], hydrothermal [59–74] and bio-inspired methods [75–78] with in-between (3) the supercritical fluids technology [79–92]. In this section a focus will be done on three of those techniques: the solid state, the sol–gel and the hydrothermal ones for the $BaTiO_3$ based materials synthesis.

### 3.1. The solid state process

The solid state process is one of the oldest and simplest synthesis route enabling the large scale production of a wide range of oxides. It consists in mixing various carbonates or oxide powders and calcined them for several hours at high temperatures (>1000 °C). In the case of $BaTiO_3$ synthesis, the barium based precursor first reacts at the surface of the titanium oxide and the reaction is propagated toward the center by diffusion to produce single phase $BaTiO_3$ particles [21].

The main strengths of this process are the low cost of the precursors and the ability to produce a large amount of material at once, however it presents some weaknesses. The final product can contain $BaCO_3$ and $TiO_2$ pollutions from unreacted precursors and a $Ba_2TiO_4$ secondary phase resulting from the high temperature reaction [49–52]. The mechanism being based on a diffusion process, the final size of the powder depends on the precursors' size and on the thermal treatment. Usually the resulting grain sizes are hundreds of nanometers with a wide size distribution. An accurate control in terms of stoichiometry within the produced material is hardly achieved, this can be critical in the case of more complex oxides such as barium strontium titanate. As a result, defects and compositional inhomogeneity can occur during further processing steps leading to a poor reliability toward materials integration into devices. To limit those drawbacks and improve the homogeneity, the different precursors have to be as small as possible and particularly well mixed. This leads, as a preliminary step, to the compulsory use of techniques such as ball milling [93–96]. The production of $BaTiO_3$ nanoparticles from $BaCO_3$ and $TiO_2$, using high energy milling applied on the precursors to obtain nanocrystals, led to the synthesis of 70 nm nanoparticles with a narrow size distribution [97]. However the remaining problems, beside the supplementary milling step, are the time duration and the occurrence of additional pollutions in the final material. Moreover, heating the powders above 1000 °C during several hours presents an important energy cost. Researches have been achieved in order to overcome those problems leading to the elaboration of versatile approaches: for example the coating of $BaCO_3$ with amorphous titania in the case of $BaTiO_3$ synthesis. This method enables a synthesis at lower temperature (around 600 °C) with a better control of the final particles size and size distribution (100–200 nm with narrow size distribution) [98]. However this

**Table 1**
Summary of the different synthesis processes with the associated material characteristics.

| Processes | Process duration | Post synthesis step | Average size (nm) | Defects | Aggregation | Homogeneity | Stoichiometry |
|---|---|---|---|---|---|---|---|
| – Dry | | | | | | | |
| Solid state | Long | Milling | >1000 | $BaCO_3$, $Ba_2TiO_4$ | Low | Low | Low |
| Molten salts | Long | Washing<br>Drying<br>Milling | >500 | $BaCO_3$ | Low | Moderate | Moderate |
| Deposition | Long | Annealing | <100 | $BaCO_3$ | Moderate | Moderate | Moderate |
| – Supercritical fluids | Short | Drying | <100 | $OH^-$ | ~Moderate | High | High |
| – Wet | | | | | | | |
| Sol–gel | Long | Drying<br>Annealing | <100 | ~$BaCO_3$, $Ba_2TiO_4$<br>$OH^-$ | Moderate | High | High |
| Hydrothermal | Moderate | Drying | 20–200 | ~$BaCO_3$<br>$OH^-$ | ~Moderate | High | High |
| Bio-inspired | Long | Drying | <100 | $BaCO_3$<br>Polymer | ~Moderate | High | High |

process is not straight forward and is still time consuming making it difficult to be industrialized [7,53,54].

### 3.2. The sol–gel process

Another main synthesis route is based on the sol–gel process which is divided in two different approaches: (1) gelation of a powder colloidal solution or (2) hydrolysis and condensation of precursors such as alkoxides or nitrate salts followed by a drying step. The first step consists in mixing the suspension of colloidal powders adjusting the pH to prevent the precipitation in the case of the approach (1) or mixing the precursors with water to start the hydrolysis of the precursors in the case (2) to produce a sol. Then, according to the targeted application, the sol can be deposited on a substrate using various methods such as spin coating or screen printing. With time the gelation of the sol appears due to the polycondensation of the colloidal powders or of the precursors. The gel is then dried to get the amorphous material and a final annealing step at 700–1000 °C is compulsory to crystallize it. It enables a better control of the produced nanoparticles in terms of size (<100 nm), stoichiometry, homogeneity and purity (slight $BaCO_3$ contamination). In this case the problem is more focused on the use of cost effective and hazardous chemicals and on the process duration. Moreover, the mandatory annealing step increases the particles size. Finally, unlike the solid state synthesis which is a dry process, the synthesis being achieved in a wet media, such materials present –OH defects [55–58]. This last point has to be carefully taken into account because it can affect the material's properties; this aspect will be presented in this paper.

### 3.3. The hydrothermal process

The hydrothermal term was introduced for geological purpose in the 1800s by Sir Roderick Murchison as the action of water at elevated temperature and pressure. The first hydrothermal system was set up in 1845 by Schafthaul to simulate the hydrothermal phenomena occurring within the earth. However it is only during the 20th century that this technology was recognized as being an important process towards material synthesis. Such reactions are mainly carried out in sealed stainless steel autoclaves heated above room temperature which consequently increases the pressure within the setup [59,60].

Usually the reaction mechanism involved in this synthesis is based on the precursors dissolution followed by a precipitation/crystallization of the product. Walton et al. were the first to follow in real time the formation of metal oxide nanoparticles in hydrothermal conditions using *in situ* neutron powder diffraction measurements. In this study they focused on the $BaTiO_3$ synthesis starting from $Ba(OD)_2$, $8D_2O$ or $BaCl_2$ precursors mixed with amorphous or crystallized $TiO_2$ particles. They were able to observe first the dissolution of the barium precursor followed by the titanium one before the crystallization of the $BaTiO_3$. As evidenced in Fig. 7 this showed that the driving force of this synthesis is based on the solubility of the less soluble precursor (here $TiO_2$) compared to the insolubility of the product ($BaTiO_3$) [61,62].

The most important parameters for those syntheses are (1) the nature and concentration of mineralizers, (2) the temperature and (3) the solvent. (1) Usually the mineralizers are alkaline hydroxides or alkaline carbonates and the most often used are the sodium or potassium hydroxides ones. According to their nature and/or concentrations they can affect the synthesis yield. It is important to be careful with the use of mineralizers because sometimes the cation can also act as a dopant in the resulting material. (2) According to the nature of the precursors, acetate or nitrate, and so the reaction mechanism, the temperature will or will not have an impact on the growth behavior. (3) Finally the type of solvents used can play an important role, the reaction occurring under pressure and temperature; the variation of those two parameters changes the fluid properties. For example the use of methanol or ethanol instead of water will change the viscosity and the thermal conductivity of the media leading to chemical reactivity variations [60,63–68].

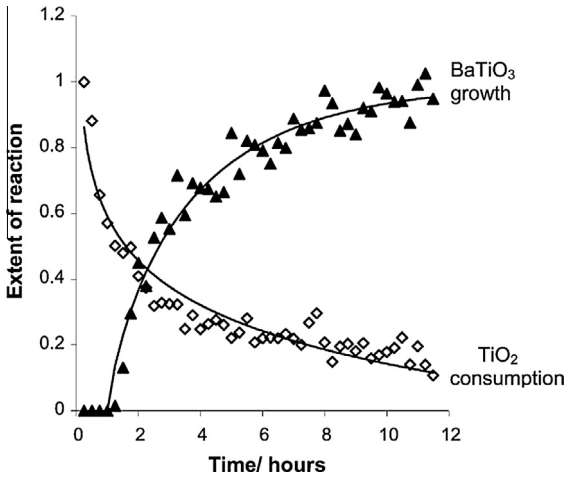


**Fig. 7.** *In situ* neutron diffraction experiment showing of the consumption of $TiO_2$ and growth of $BaTiO_3$ with time 'Reprinted from ref. [61] Copyright © (2001), American Chemical Society'.

This technology presents different advantages: (1) it enables the synthesis of various kinds of metal oxide nanoparticles with a good control over their size (from few to several nanometers), size distribution and morphology, at temperatures and pressures below 200 °C and 1.5 MPa respectively, (2) it is environmentally friendly because the solvents are generally not hazardous and the operating temperature is low (<200 °C) and (3) it is low cost and reliable so it is possible to scale up this technology toward industrial production. However in some cases the apparition of a slight $BaCO_3$ contamination is observable. In addition, as in the case of the sol–gel process, the reaction being achieved in a wet media, the presence of –OH defects is reported [60,65,69–74].

Each of these processes present different strengths and drawbacks which are limiting to fulfill the materials' down scaling expectations (Table 1). That is why it is necessary to develop new synthesis processes such as the supercritical fluid technology in order to suitably answer the demand.

## 4. The supercritical fluid technology, an alternative

The supercritical fluid technology can be considered as an extension of the usual synthesis routes, coupling advantages of the "conventional" methods with some additional inputs making it even more attractive. One of the most valuable one is the enhancement of the chemical reactivity leading to a fast synthesis (tens of second) enabling the use of continuous processes favoring the scaling up ability toward industry.

### 4.1. What is a supercritical fluid?

#### 4.1.1. General consideration

A supercritical fluid is a single phase domain which appears crossing the critical pressure and temperature of the considered fluid. For example in the case of water (Fig. 8) this domain appears for pressures over 22.1 MPa and temperatures higher than 374 °C.

It is important to know that the supercritical domain is not a proper phase; it is a continuous change from the liquid phase to the gas one. Varying the pressure and temperature it is possible

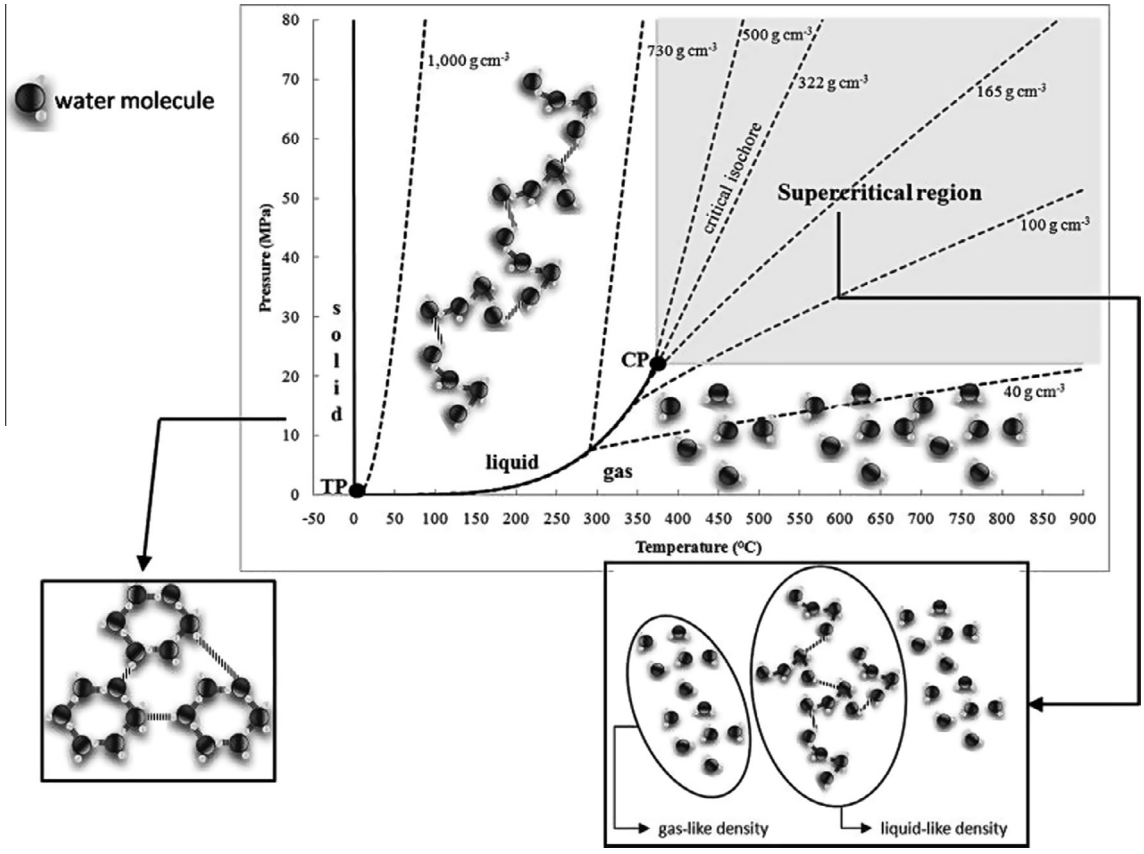


**Fig. 8.** Pressure–temperature phase diagram of pure water. TP is the triple point ($T_{TP}$ = 0 °C, $P_{TP}$ = 612 Pa) and CP is the critical point ($T_{CP}$ = 374 °C, $P_{CP}$ = 22.1 MPa). Some isochoric curves are drawn (dotted lines) 'Reprinted from ref. [103] Copyright © (2010), Society of Chemical Industry'.

to adjust the density, viscosity, diffusivity or surface tension of the media leading to the apparition of very interesting properties not only for the materials synthesis [79,80,82,84,86,88,99–101] but also for their recycling [102]. To summarize, this domain combines some properties of the liquid phase to the ones of the gas phase [103].

### 4.1.2. Case of mixtures

In the case of mixtures the interactions between the molecules of different nature induce the modification of some properties such as the critical pressure and temperature. Those properties are then going to be specific to a given mixture at a well-defined composition. For example in the case of water/ethanol mixtures, interesting in the case of the ferroelectric nanomaterials synthesis, the polarity of each species will generate hydrogen bonding between the two types of molecules: the ethanol molecules are going to affect the water molecules structure leading to changes on the critical pressure and temperature of the mixture [104]. In Fig. 9 Bazaev et al. [105] combined theoretical and experimental data from literature [106–108] in order to predict the critical temperature and pressure for a given water/ethanol mixture composition.

The different studies concerning the critical temperatures evolution with the media composition were in very good agreement. Concerning the critical pressures, except the study of Griswold et al. [107] assuming a linear evolution, the different results were also in good agreement.

## 4.2. Principle of the nanomaterials synthesis in supercritical fluids

Even if the supercritical domain is known for a long time it is only in the early 90s that Prof. Tadafumi Adschiri first reported

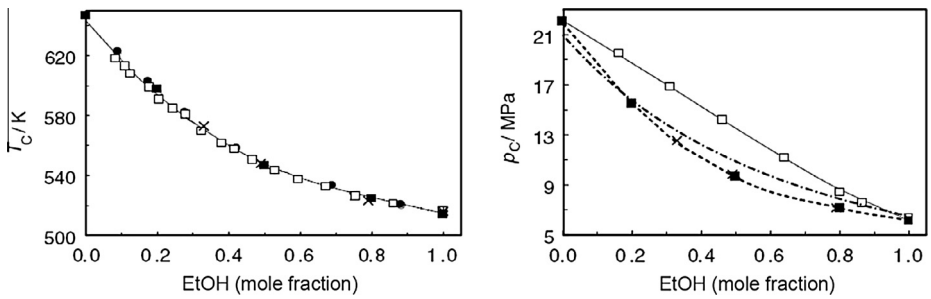


**Fig. 9.** Evolution of the critical pressures and temperatures according to water/ethanol mixture composition where: ● Marshal et al. [106], □ Griswold et al. [107], ×Barr-David et al. [108], ■ Bazaev et al. [105]' Adapted from ref. [105] Copyright © (2007), Elsevier'.

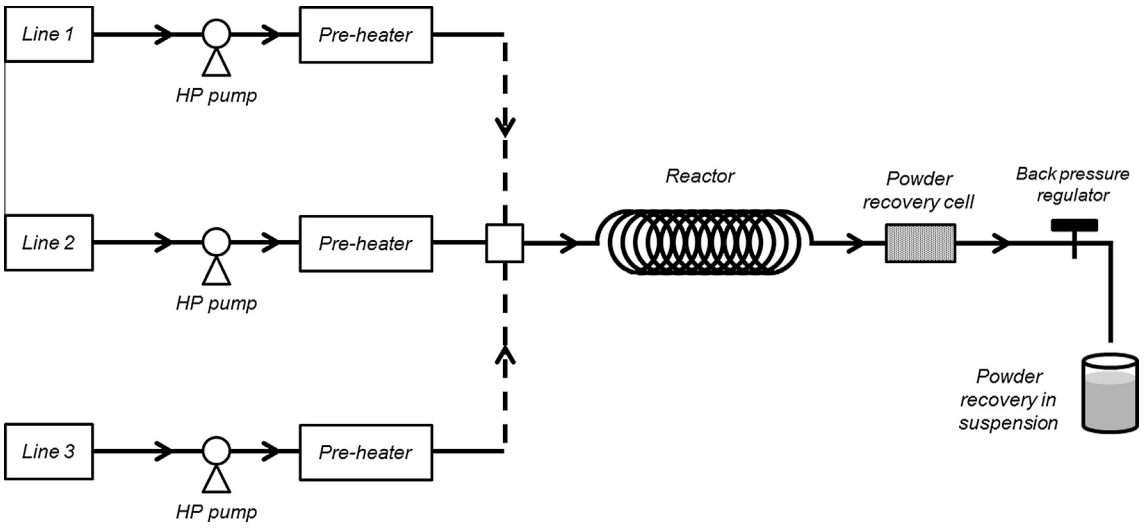


**Fig. 10.** General sketch of the supercritical fluid process.

the synthesis of metal oxide nanoparticles using supercritical water with the synthesis of cerium oxide nanoparticles [109].

The main concept of such setup (Fig. 10) is a reactor fed with high pressure pumps and pressurized with a back pressure regulator valve. The produced material can be recovered whether as a powder using a particle filter positioned before the back pressure regulator valve or in suspension at the outlet of the process.

This type of setup is very flexible and can be tuned at will. In its simplest configuration the process will present a single line to inject the precursors dissolved into the solvent. For example Slostowski et al. [110] synthesized cerium oxide from ammonium cerium(IV) nitrate solubilized in different alcohols. In this case the heat was only increased by the heating system of the reactor. It can be more complex, for example Hakuta et al. developed another design to produce cerium oxide adding a second preheated line [111]. The first line feeding the reactor with the precursors and the second one bringing preheated solvent to the reactor. The two flows are mixed at the inlet of the reactor. There the heating is mainly done by the solvent line. The heating system of the reactor is mainly used to keep the temperature. In other cases the setup can present several lines according to the nature of the precursors and their solubility in the solvents used [88,91] or to make more complex structures like hybrids [112,113].

According to the nature of the reagents and solvents used, there are four main kinds of chemical reactions which can occur in supercritical conditions: (1) hydrothermal reaction of metal nitrates or metal–organic precursors in supercritical water leading to their hydrolysis and dehydration [79,80,86,114–116], (2) the thermal decomposition of metal–organic precursors [84,117,118], (3) the reduction/oxidation reactions of metal salts or metal–organic precursors [119–124] and (4) the hydrolysis/condensation reactions known as sol–gel [91,125,126]. Adjusting the experimental conditions such as the reactor's pressure and temperature, the nature of the precursors and their concentration, the type of solvents and the residence time within the reactor, it is then possible to control the inorganic or hybrids (inorganic/organic) nanoparticle design in terms of size, morphology, structure, composition, crystallinity and surface properties [82,101].

### *4.3. Interest of the supercritical fluid technology for nanoparticles synthesis*

This specific region of the phase diagram exhibits very interesting properties which are intermediate between liquid and gas phases. The solubility of the precursors being dependent on the density of the solvent, it is easy to optimize it changing the pressure and temperature. In addition its gas like viscosity and diffusivity increases the mass and heat transfers making the reaction kinetics faster [92]. A very important aspect is the possibility to use this technology as a continuous process to synthesize in a single step high quality nanomaterials (well crystallized, narrow size distribution, pure, stoichiometric, etc.) in only few seconds and with a good reliability [127].

This technology is also versatile enabling a controlled synthesis of various kinds of nanoparticles such as metals (Cu, Ag, Pt, Pd, etc.) [120–124,128–133], oxides ($Ba_xSr_{1-x}TiO_3$ with $0 \leqslant x \leqslant 1$, $TiO_2$, $ZrO_2$, $CeO_2$, $Fe_2O_3$, $Cu_2O$, $Cr_2O_3$, $Al_2O_3$, ZnO, etc.) [91,118,125–127,133–139], nitrides ($Ni_3N$, $Cu_3N$, $Co_2N$, $Cr_2N$, $Fe_4N$, etc.) [118] and more complex structures such as core shell particles [140,141]. In those conditions of synthesis the nucleation is favored over the growth leading to the production of powder with high specific surface area which can be very interesting for catalysis or gas capture [142].

This sustainable process operates at relatively low temperature (<400 °C) and mainly uses green solvents such as water or alcohols. Finally, it is a scalable technology toward industrial production and the first commercial plant is already running producing 1000 tons per year of $LiFePO_4$ [143].

All those aspects lead to a good compromise between the solid state and the sol–gel syntheses and enhance the hydrothermal one. On one side it enables the production of a large amount of material in a reasonable duration like in the case of the solid state process. On the other it offers a good control on the synthesized particles in terms of size, size distribution, composition, purity and crystallinity characteristic of the wet syntheses. In addition it fits with an environmentally friendly policy through the use of green solvents and the moderate amount of energy needed [18,143].

In the next part, the advantages concerning the quality of the produced materials will be presented and illustrated through the example of the $BaTiO_3/Ba_xSr_{1-x}TiO_3$ (with $0 \leqslant x \leqslant 1$) nanoparticles synthesis.

## 5. Supercritical fluid synthesis of barium strontium titanate nanoparticles

Only few papers (around 10) report the synthesis of $BaTiO_3$ material in supercritical fluids and are mainly shared between two research groups, the supercritical fluid research center at the

national institute of advanced industrial science and technology (AIST – Senday – Japan) and the supercritical fluid group at the institute of condensed matter chemistry of Bordeaux (ICMCB – CNRS – France). From those 10 papers two main approaches are presented toward the synthesis of $BaTiO_3$ based nanoparticles in supercritical fluids: (1) the "supercritical hydrothermal like synthesis" based on hydroxide ($Ba(OH)_2$), oxide ($TiO_2$) or nitrate ($Ba(NO_3)_2$) precursors or (2) the "supercritical sol–gel like synthesis" based on alkoxides precursors which not only enables to synthesis $BaTiO_3$ (as in the case (1)) but also the barium strontium titanate (BST – $Ba_{1-x}Sr_xTiO_3$ with $0 \leqslant x \leqslant 1$) entire solid solution one.

### 5.1. Supercritical hydrothermal synthesis of barium titanate

Hayashi et al. reported the continuous synthesis of $BaTiO_3$ in supercritical water based on different types of precursors ($Ba(NO_3)_2$, $Ba(OH)_2$ and $TiO_2$). For these syntheses they chose the setup configuration where a preheated line of water is used to heat the media in order to faster the reaction when it is mixed with the precursors at the inlet of the reactor [88]. The precursor line is not preheated to avoid side reactions. The $BaTiO_3$ crystallizes inside the reactor which is under supercritical conditions and the powders are recovered after the back pressure regulator.

One type of precursors was a mixture of $TiO_2$ nanoparticles dispersion with a solution of $Ba(OH)_2$. According to the flow rate, the conditions of pressure and temperature, the nanoparticles were produced in time ranging from few milliseconds to tens of seconds. The $BaTiO_3$ nanoparticles average size was comprised between 10 and 50 nm and increasing the mean size increased the size distribution. In the case of 50 nm particle size the distribution was spread from 10 to 150 nm exhibiting aggregated particles with high crystallinity. According to the conditions of pressure and temperature, the crystal phase changed from the cubic to the tetragonal one. To get a tetragonal phase, the temperatures ranged from 400 to 420 °C and the pressure from 20 to 35 MPa. Although the produced nanoparticles were pure, the presence of –OH defects was pointed out.

Two reaction mechanisms similar to the most well-known ones of hydrothermal syntheses were proposed [62]: (1) dissolution of $TiO_2$ precursor followed by crystallization of $BaTiO_3$ as demonstrated by Walton et al. [61] or (2) *in situ* crystallization based on barium diffusion into $TiO_2$ nanocrystals [81,85,87,90].

$BaTiO_3$ was also obtained mixing $Ba(NO_3)_2$ with a dispersion of $TiO_2$ nanocrystals and using a residence time of 8 ms leading to nanoparticles of 10 nm with narrow size distribution. The particles were well crystallized but aggregated and in the cubic phase. Again the presence of –OH defects was detected. In this case, the proposed mechanism was based on the hydrolysis and precipitation of the precursors [89,112].

The use of these types of precursors only leads to the synthesis of $BaTiO_3$ nanopowder. However, as presented in the following part, the use of alkoxides enables the production of barium strontium titanate nanopowders over the entire solid solution.

### 5.2. Supercritical sol–gel like synthesis of barium strontium titanate

Bocquet et al. were the first to report the synthesis of $BaTiO_3$ starting with a double alkoxide ($BaTi(O\text{-}iC_3H_7)_6$) in supercritical water/isopropanol mixture [83]. In this study the didn't used an extra preheated line and the temperature was only fixed by the heating system on the reactor. However, because the alkoxides are not stable in water, two lines were used: one for the precursors dissolved in isopropanol, the other for a mixture of isopropanol and water. The reactor was divided in two parts: the first one was in liquid phase to hydrolyze the alkoxides and the second one in supercritical conditions to thermally treat the produced nanoparticles. These nanoparticles presented an average size of 10 nm with a narrow size distribution and a specific surface of 80–90 $m^2/g$. The infra-red measurements showed –OH defects.

Based on those results, Reverón et al. combined both syntheses using alkoxide precursors reacting in water/alcohol mixtures and a preheated line. They first synthesized $BaTiO_3$ nanopowder then demonstrated for the first time the synthesis of the entire solid solution of BST nanoparticles in supercritical fluids [91,125,126,144].

Barium, strontium and titanium isopropoxides were dissolved in ethanol. The flow reaction system was made of two injection lines: one for the precursors dissolved in ethanol and the second one for water in order to proceed to the hydrolysis of the precursors. The entire system was pressurized at 26 MPa using a back pressure regulating valve. The water line was preheated at 150 °C to faster the reaction, however the injection line of precursors was kept at room temperature to avoid side reactions. The two lines were mixed at the inlet of a height meter length tubular reactor with 16 $cm^3$ of inner volume. The first four meters were heated at $T_1$ = 150 °C to enhance the hydrolysis of the precursors and the four last meters were heated at $T_2$ = 380 °C above the critical point of the water/ethanol mixture to promote the crystallization. Using this setup the experimental parameters were tuned for the $BaTiO_3$ synthesis [91]. One of the most important parameter, beside the pressure and temperature, was the ethanol molar ratio. For an ethanol molar ratio of 0.29 pure $BaTiO_3$ nanoparticles with a crystallinity higher than 90% were obtained. The particles presented an average size of 41 nm with a size distribution of 13 nm. For all the materials the presence of –OH defects was detected.

After the optimization of the experimental conditions for $BaTiO_3$ synthesis, the process was transferred to $Ba_{1-x}Sr_xTiO_3$ (with $0 \leqslant x \leqslant 1$) solid solution synthesis [125,126]. Increasing the strontium amount leads to a decrease of the mean particle size. As showed in Fig. 11 the average size went from 41 ± 13 nm in the case of $BaTiO_3$, to 25 ± 6 nm for $x$ = 0.5 and to 19 ± 5 nm in the case of $SrTiO_3$.

Those materials were then uniaxially pressed into pellets and sintered 4 four hours at 1325 °C in order to measure their ferroelectric properties [125,144]. The variation of the $T_{Curie}$ according to the powder composition (strontium content) was in agreement with the literature (Fig. 11) exhibiting the synthesis accuracy in terms of materials composition and stoichiometry.

The relationship between the size variation and the composition of the synthesized nanoparticles being unclear, Philippot et al. [138] performed a deep study on the nucleation and growth of those particles synthesized in similar experimental conditions. The precursors were the same (alkoxides) as well as the ethanol molar ratio (0.29) however the reaction was achieved in a 24 m reactor length pressurized at 23 MPa and heated at a temperature of 400 °C giving a residence time close to one minute. Fig. 12 confirms the quality of the material in terms of particle crystallinity as well as the trend concerning the size variation according to the composition (from 20 nm ± 6 nm for $BaTiO_3$ to ± 16 nm ± 2 nm for $Ba_{0.6}Sr_{0.4}TiO_3$).

To understand this behavior, *in situ* synchrotron powder diffraction was coupled with *ex situ* analyses such as Fourier transform infrared spectroscopy (FTIR), Raman spectroscopy, X-ray photoelectron spectroscopy (XPS), X-ray diffraction (XRD) and high resolution transmission electron microscopy (HR-TEM). The *in situ* analyses confirmed the influence of the strontium substitution on the nanoparticles growth. The *ex situ* analysis evidenced the presence of surface –OH defects which decrease when increasing the barium substitution with strontium. Those defects were identified as resulting from the dissolution of the barium and strontium. However, the ionic bond Ba–O being considered as weaker than

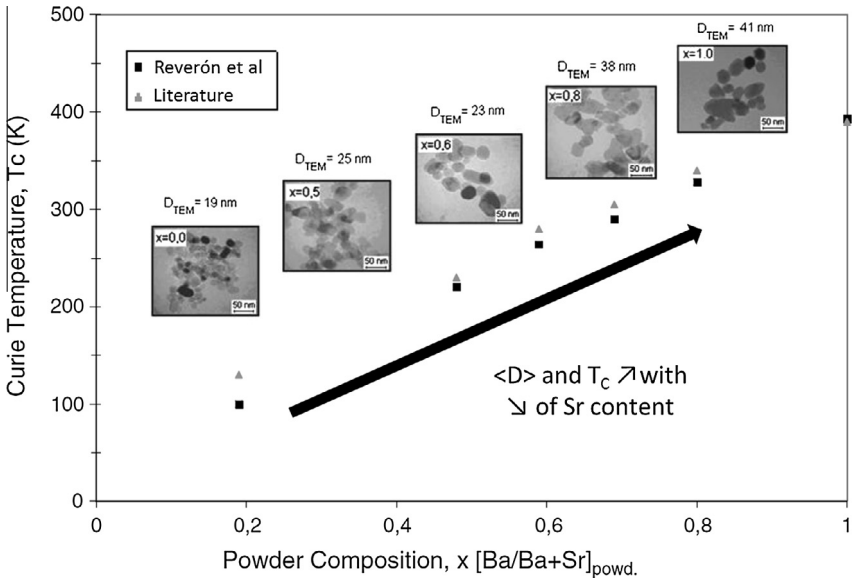


**Fig. 11.** Effect of barium substitution with strontium on particles size and Curie temperature $T_C$ 'Adapted from ref. [125] Copyright © (2006), IOP Publishing'.

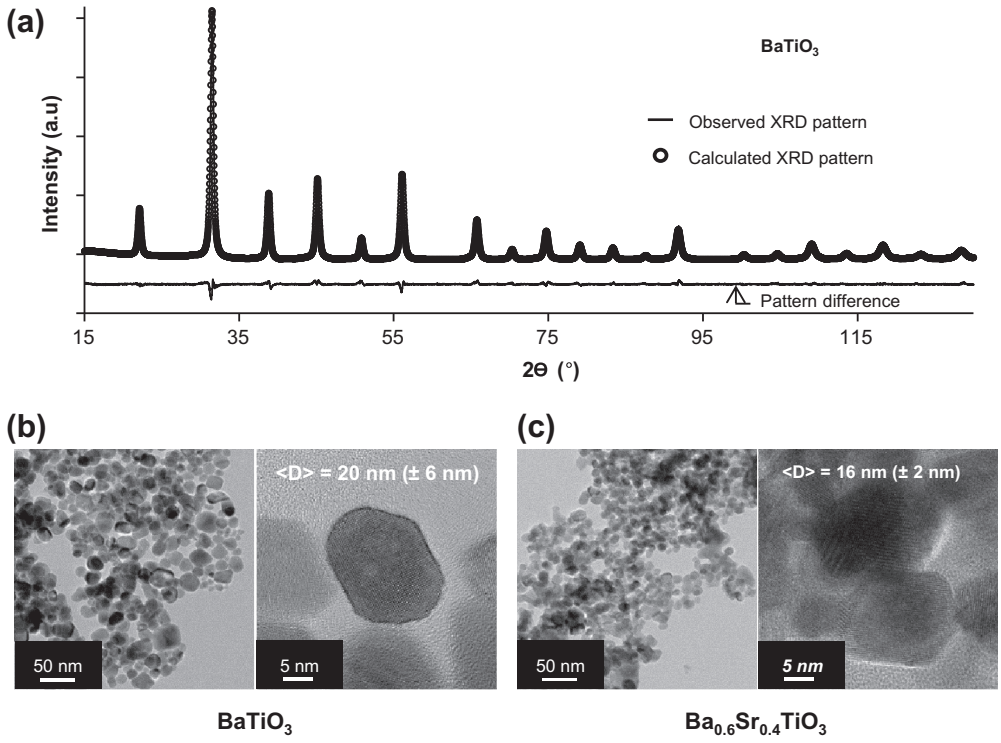


**Fig. 12.** Continuous synthesis of BT – BST from alkoxides in supercritical water/ethanol mixture. BT synthesis: (a) Rietveld refinement, (b) HR-TEM pictures of $BaTiO_3$, (c) HR-TEM pictures of $Ba_{0.6}Sr_{0.4}TiO_3$ 'Adapted from ref. [138] Copyright © (2014), Elsevier'.

the Sr–O one [145–148], the increase of strontium content will decrease the amount of dissolved ions. This will decrease the density of surface –OH defects. The synthesis mechanism being identified as following a sol–gel chemistry, the decrease of surface –OH will decrease the ability of the precursor to react at the surface of the particles and thus, limits the growth. Structural –OH defects were also identified and tended to decrease with the increase of strontium as well as the disorder due to titanium off centering at this size range.

Although this process enables the synthesis of high quality and well crystallized nanoparticles with narrow size distribution, there are still just few papers reporting the supercritical synthesis of $BaTiO_3$ or BST nanomaterials. Two main synthesis routes can be used according to the nature of the precursors leading to different reaction mechanisms. The one based on alkoxide precursors enables more flexibility than the other with the possibility to produce the entire solid solution between $BaTiO_3$ and $SrTiO_3$ ($Ba_{1-x}Sr_xTiO_3$ with $0 \leqslant x \leqslant 1$). In both cases it is important to note that even if

the syntheses are achieved under pressure (around 25 MPa) it is too low to have any consequences on the material's structure (Fig. 5).

Those materials fulfilling a part of the processing requirements, the next section will describe their properties.

## 6. Discussion

It is critical to control and understand the link between the structure and the ferroelectric properties of the material. To do that different analyses were achieved [138]. In the following part the results are compared to the literature in order to conclude on their crystal structure and defects.

### 6.1. Study of the nanoparticles crystalline phase

#### 6.1.1. XRD analysis

In the framework of our work (Fig. 12a) the XRD analysis points a cubic structure at room temperature. However the $BaTiO_3$ structure is supposed to be tetragonal and the XRD pattern should exhibit a splitting of the (002)/(200) peak at $2\theta \approx 45°$. Decreasing the nanoparticles size down to tens of nanometers, the splitting is no longer observable. According to Fig. 13, in the case of $BaTiO_3$ synthesized by precipitation, it is restored for nanoparticles reaching a size around 200 nm [149].

The cubic state of the particles of few tens of nanometers could also be confirmed by differential scanning calorimetry (DSC) measurements [132–136].

#### 6.1.2. Raman analysis

Contrary to the XRD analysis which represents an average response, the Raman technique enables a much more localized analysis. It is a very sensitive tool suitable to characterize crystal structures and phase transitions. It detects the local dynamic symmetry in small regions (coherence length lower than 2 nm) making it useful to prove non centrosymmetric local structure in apparent pseudo-cubic nanopowders.

The Raman analysis of the $BaTiO_3$ nanoparticles we produced is presented in Fig. 14. It exhibits the optical modes at ≈ 305, 520 and 720 $cm^{-1}$ characteristic of the tetragonal phase among other active modes at: 180, 270, 480 and 810 $cm^{-1}$. This is in agreement with other reports where the same active modes were identified [150–152].

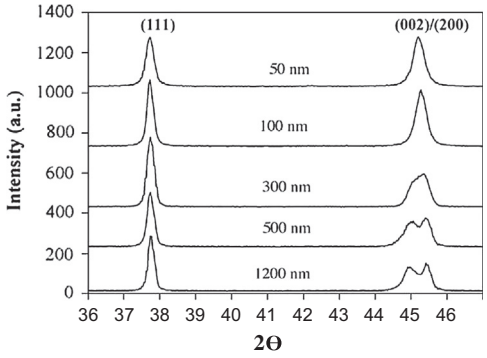


**Fig. 13.** $BaTiO_3$ particles size effect on XRD pattern 'Adapted from ref. [149] Copyright © (2006), Elsevier'.

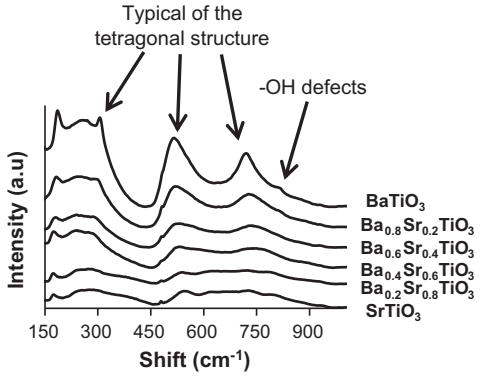


**Fig. 14.** Raman analysis of BST solid solution synthesized in supercritical fluids 'Adapted from ref. [138] Copyright © (2014), Elsevier'.

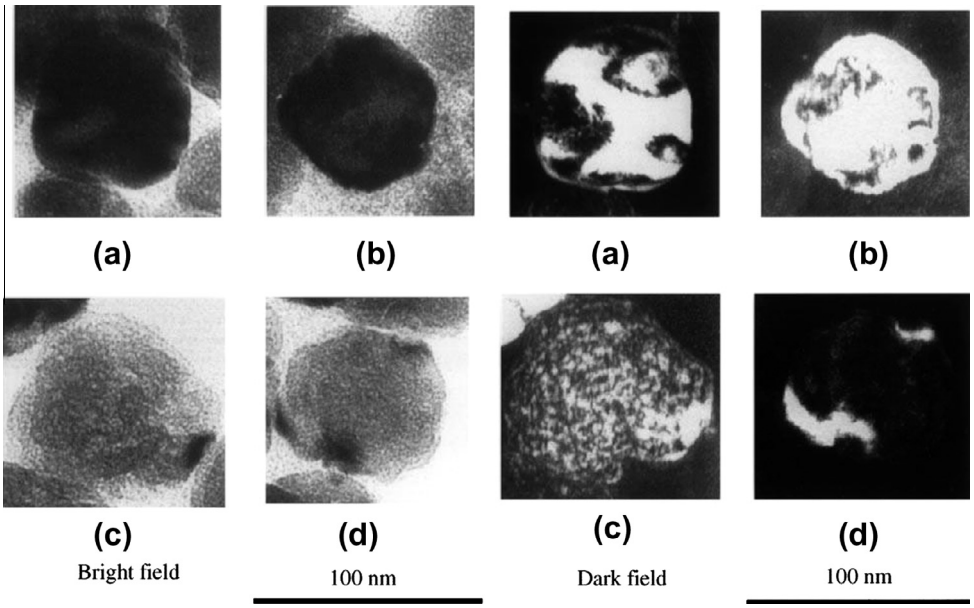


**Fig. 15.** TEM bright and dark field images of four individual BT nanocrystals with different contrasts: (a) nearly half-bright color and half-dark color contrast; (b) bright color dominant contrast; (c) equal bright-dark color contrast with nearly homogeneous distribution; and (d) dark color dominant contrast 'Reprinted from ref. [153] Copyright © (2000), Elsevier'.

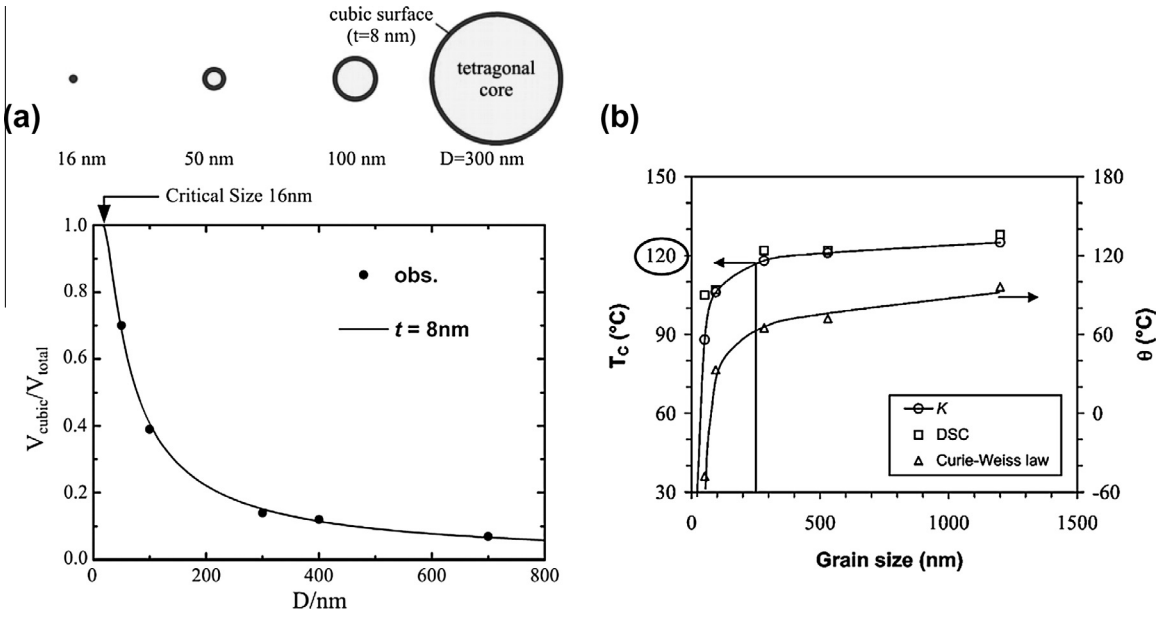


**Fig. 16.** $BaTiO_3$ grain size effect on (a) the volume ratio of the cubic component to the entire $BaTiO_3$ nanopowder at 300 K, $V_{cubic}/V_{total}$ and (b) $T_{Curie}$ 'Adapted from ref. [31,58] Copyright © (2005), Akadémiai Kiadó, Budapest and Copyright © (2004), American Physical Society'.

As reported by Smith et al. [28], a part of the other active modes observable (180, 270 and 480 $cm^{-1}$) can be attributed to some structural disorder such as titanium off centering. This off centering is associated to a high surface strain applied within the structure for particles at this size range. The disorder is illustrated Fig. 15 with the use of dark and bright field transmission electron microscopy (TEM) pictures. There, the variations of contrast across a single particle correspond to a variation of strain within it [153].

In addition it was observed in Fig. 14 a decrease of the intensities of the peaks corresponding to the tetragonal phase at room temperature while increasing the strontium amount. This is in agreement with the literature showing a decrease of the phase transition temperature from cubic to tetragonal toward room temperature increasing the strontium amount [23]. This observation confirms the presence of a tetragonal phase.

Combining this conclusion with the one based on XRD and DSC analyses enables to demonstrate a coexistence of the cubic and tetragonal phases at the nanoscale. Based on the core shell model, the next section presents how these two phases are organized inside the particles.

### 6.2. Core–shell model

The identified strain within the nanoparticles of such size leading to changes in the domains structure is going to reduce the displacement ability of the titanium in the cell [28–30]. This is a critical parameter concerning the intrinsic properties of the material; since it will block the phase transitions and decrease the ferroelectric properties.

Moreover the Raman analysis Fig. 14 pointed the presence of –OH defects (optical mode at 810 $cm^{-1}$) which tends to decrease with the increase of strontium molar ratio. The presence of those defects is characteristic of wet synthesis routes like the sol–gel [154–156], the hydrothermal [14,15,32,153,157,158] or the supercritical [88–91,125] processes. They lead to the creation of barium vacancies at the surface of the particles in order to maintain the electroneutrality of the structure [159,160]. This stabilizes a cubic phase at the surface of the particles [161] leading to the core–shell model: the core of the particle being tetragonal, surrounded with a cubic shell also called "dead layer" [13,31,32]. Some papers propose more complex development of this theory with a notion of double layer. The core of the particles being tetragonal and the external shell cubic with in between a gradient of lattice strain layer (GLSL) presenting a gradient of tetragonality [33,34].

As presented in Fig. 16a, the size of the particles decreasing, the proportion of the cubic shell increases compared to the tetragonal core leading to a progressive loss of the ferroelectric behavior [13,31–34].

The notion of critical size in terms of particle dimensions was then introduced corresponding to a decrease of the tetragonal structure with the nanoparticles size (Fig. 16b) [12,13,15,32,153,157,162]. Many theoretical and experimental researches have been carried out in order to define this critical size but they led to contradictory results predicting critical sizes going from few nanometers to several tens of nanometers [10,26,153,58,163–165]. These differences highlight the influence of both the synthesis and sintering conditions.

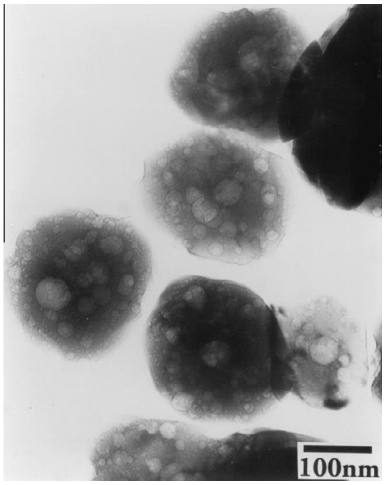


**Fig. 17.** HR-TEM picture of hydrothermal $BaTiO_3$ heat-treated for 2 h [166].

In the following, the processing of such particles toward electronic applications and the issues which have to be overcome are discussed and illustrated with the example of MLLCs manufacturing.

### 6.3. Nanoparticles processing

The processing of those nanoparticles into dense and homogeneous thin films can introduce defects which can be critical especially for MLCCs application. Heating the films up to 800 °C is going to suppress the –OH defects releasing water and leading to the apparition of pores (Fig. 17). Those pores are going to migrate at the grain boundaries thanks to the grain growth. In the case of MLCCs those pores will then be accumulated at the interface between the film and the inner electrodes leading to the apparition of the so called "bloating effect" [166].

To avoid this effect, a preliminary step of dehydration is going to be compulsory to produce high quality components. In the case of single thin film this aspect is less critical because an annealing step can be achieved before the top layer deposit, enabling the pores to be released 'Reprinted from ref. [167] Copyright © (2004), John Wiley and Sons'.

## 7. Conclusion

The perovskite $BaTiO_3$ system has been gaining a lot of attention for decades thanks to its high dielectric permittivity. Due to the new expectations from the industry in terms of materials quality (size, crystallinity, purity, and homogeneity), amount of production, cost and environment, the main synthesis routes reach their limits. New processes have to be developed and the route based on the supercritical fluid technology is especially promising. In addition to bring an answer to the materials' quality expectations, this scalable technology enables a fast and reliable production using green solvents and for a moderate energy cost. Moreover this technology is versatile and not only enables the production of oxide nanoparticles but also metals, nitrides and more complex structures such as core shell ones. The example of the $BaTiO_3$ synthesis is really well illustrating the contribution which can be brought by this technology to the industrial production of metal oxide nanomaterials. In tens of second, well crystallized $BaTiO_3$ nanoparticles of 20 nm with a narrow size distribution (±6 nm) are produced. However, reaching this size range tends to impact the material ferroelectric properties. This leads to a critical size where the nanoparticles are no longer tetragonal, illustrated with the core–shell model. In addition, the presence of –OH defects must be carefully taken into account for the processing and integration steps of those materials into devices due to their direct impact on the final performances.

The challenge is now to be able to produce dense ceramics with those nanoparticles keeping their grain size in order to characterize their intrinsic ferroelectric properties. Even if noticeable progresses have been achieved, at the current state of the art, this aim is not reached. However the use of fast sintering technologies such as spark plasma sintering is promising and could enable to face this challenge.

## Author Contributions

The paper was written through contributions of all authors. All authors have given approval to the final version of the paper.

## Acknowledgment

The authors acknowledge the IDS FunMat European doctoral school and the Region Aquitaine for their financial support.

## References

[1] J. Curie, P. Curie, Développement par pression de l'électricité polaire dans des crystaux hémiédriques à faces inclinées, Comptes Rendus de l'Académie Des Sciences (1880) 294–295.
[2] D. Brewster, Observation on the Pyro-Electricity in minerals, Edinburgh J. Sci. 1 (1824) 208–218.
[3] G. Busch, P. Scherrer, Eine neue seignette-elektrische Substanz, Naturwissenschaften 23 (1935) 737.
[4] J. Valasek, Piezoelectric and allied phenomena in Rochelle salt, Phys. Rev. (1920) 537.
[5] E. Schrödinger, Studien über Kinetik der Dielektrika, dam Schmelzpunkt, Pyro-und Piezoelektrizität, S.B. Akad. Wiss. Wien. (1912) 1937–1972.
[6] L.E. Cross, R.E. Newnham, History of Ferroelectrics, in: E. Lense (Ed.), Ceramics and Civilization, Volume III: High Technology Ceramics: Past, Present, and Future: the Nature of Innovation and Change in Ceramic Technology, The American Ceramic Society, 1987: pp. 289–305.
[7] G.H. Haertling, Ferroelectric ceramics: history and technology, J. Am. Ceram. Soc. 82 (1999) 797–818.
[8] R. López-juárez, F. González, M.-E. Villafuerte-Castrejón, Lead-free ferroelectric ceramics with perovskite structure, in: M. Lallart (Ed.), Ferroelectrics – Material Aspects, InTech, Rijeka, 2011, pp. 305–330.
[9] B.M. Wul, I.M. Goldman, Dielectric constants of titanates of metals of the second group, Doklady Akademii Nauk SSSR (1945) 139–142.
[10] T.-C. Huang, M.-T. Wang, H.-S. Sheu, W.-F. Hsieh, Size-dependent lattice dynamics of barium titanate nanoparticles, J. Phys.: Condens. Matter 19 (476212) (2007) 1–12.
[11] M. Lallart, Ferroelectrics – Applications, InTech, Rijeka, 2011.
[12] L. Huang, Z. Chen, J.D. Wilson, S. Banerjee, R.D. Robinson, I.P. Herman, et al., Barium titanate nanocrystals and nanocrystal thin films: synthesis, ferroelectricity, and dielectric properties, J. Appl. Physicsp. 100 (034316) (2006) 1–10.
[13] S. Wada, T. Hoshina, K. Takizawa, M. Ohishi, H. Yasuno, H. Kakemoto, et al., Origin of ultrahigh dielectric constants for barium titanate nanoparticles, J. Korean Phys. Soc. 51 (2007) 878.
[14] X. Zhu, Z. Zhang, J. Zhu, S. Zhou, Z. Liu, Morphology and atomic-scale surface structure of barium titanate nanocrystals formed at hydrothermal conditions, J. Cryst. Growth 311 (2009) 2437–2442.
[15] X. Zhu, J. Wang, Z. Zhang, J. Zhu, S. Zhou, Z. Liu, et al., Atomic-scale characterization of barium titanate powders formed by the hydrothermal process, J. Am. Ceram. Soc. 91 (2008) 1002–1008.
[16] Y. Zhang, X. Wang, Z. Tian, K.-H. Hur, L. Li, Preparation of BME MLCC powders by aqueous chemical coating method, J. Am. Ceram. Soc. 94 (2011) 3286–3290.
[17] Y. Zhang, X. Wang, J. Kim, J.-R. Kim, K.-H. Hur, L. Li, Uniform coating of $BaTiO_3$–$Dy_2O_3$–$SiO_2$ compound nano layer on Ni particles for MLCC electrode, J. Am. Ceram. Soc. 96 (2013) 2163–2166.
[18] J.A. Dahl, B.S. Maddux, J.E. Hutchison, Toward greener nanosynthesis, J. Chem. Rev. 107 (2007) 2228–2269.
[19] J. Varghese, R.W. Whatmore, J.D. Holmes, Ferroelectric nanoparticles, wires and tubes: synthesis, characterisation and applications, J. Mater. Chem. C 1 (2013) 2618.
[20] D. Damjanovic, Ferroelectric, dielectric and piezoelectric properties of ferroelectric thin films and ceramics, Rep. Prog. Phys. 61 (1998) 1267–1324.
[21] D. Yoon, Tetragonality of barium titanate powder for a ceramic capacitor application, J. Ceram. Process. Res. 7 (2006) 343–354.
[22] M.-J. Pan, C.A. Randall, A brief introduction to ceramic capacitors, IEEE Electr. Insul. Mag. 26 (2010) 44–50.
[23] H. Frayssignes, B.L. Cheng, G. Fantozzi, T.W. Button, Phase transformation in BST ceramics investigated by internal friction measurements, J. Eur. Ceram. Soc. 25 (2005) 3203–3206.
[24] T. Ishidate, S. Abe, H. Takahashi, N. Môri, Phase diagram of $BaTiO_3$, Phys. Rev. Lett. 78 (1997) 2397–2400.
[25] S. Yoon, J. Dornseiffer, Y. Xiong, D. Grüner, Z. Shen, S. Iwaya, et al., Spark plasma sintering of nanocrystalline $BaTiO_3$-powders: consolidation behavior and dielectric characteristics, J. Eur. Ceram. Soc. 31 (2011) 1723–1731.
[26] S. Lin, T. Lü, C. Jin, X. Wang, Size effect on the dielectric properties of $BaTiO_3$ nanoceramics in a modified Ginsburg-Landau-Devonshire thermodynamic theory, Phys. Rev. B 74 (134115) (2006) 1–5.
[27] V. Hornebecq, C. Huber, M. Maglione, M. Antonietti, C. Elissalde, Dielectric properties of pure $(BaSr)TiO_3$ and composites with different grain sizes ranging from the nanometer to the micrometer, Adv. Funct. Mater. 14 (2004) 899–904.
[28] M.B. Smith, K. Page, T. Siegrist, P.L. Redmond, E.C. Walter, R. Seshadri, et al., Crystal structure and the paraelectric-to-ferroelectric phase transition of nanoscale $BaTiO_3$, J. Am. Chem. Soc. 130 (2008) 6955–6963.
[29] T. Hoshina, K. Takizawa, J. Li, T. Kasama, H. Kakemoto, T. Tsurumi, Domain size effect on dielectric properties of barium titanate ceramics, Jpn. J. Appl. Phys. 47 (2008) 7607–7611.
[30] C. Fang, L. Chen, Study of ferroelectric nanodomains and the effect of grain size in $BaTiO_3$ ceramics, Philos. Mag. Lett. 92 (2012) 37–41.
[31] S. Aoyagi, Y. Kuroiwa, A. Sawada, H. Kawaji, T. Atake, Size effect on crystal structure and chemical bonding nature in $BaTiO_3$ nanopowder, J. Therm. Anal. Calorim. 81 (2005) 627–630.

[32] H.-W. Lee, S. Moon, C.-H. Choi, D.K. Kim, Synthesis and size control of tetragonal barium titanate nanopowders by facile solvothermal method, J. Am. Ceram. Soc. 95 (2012) 2429–2434.
[33] C. Fang, D. Zhou, S. Gong, Core–shell structure and size effect in barium titanate nanoparticle, Physica B 406 (2011) 1317–1322.
[34] T. Hoshina, Size effect of barium titanate: fine particles and ceramics, J. Ceram. Soc. Jpn. 121 (2013) 156–161.
[35] A. Schilling, S. Prosandeev, R.G.P. McQuaid, L. Bellaiche, J.F. Scott, J.M. Gregg, Shape-induced phase transition of domain patterns in ferroelectric platelets, Phys. Rev. B 84 (064110) (2011) 1–5.
[36] K. Suzuki, K. Kijima, Well-crystallized barium titanate nanoparticles prepared by plasma chemical vapor deposition, Mater. Lett. 58 (2004) 1650–1654.
[37] K. Suzuki, K. Kijima, Size driven phase transition of barium titanate nanoparticles prepared by plasma chemical vapor deposition, J. Mater. Sci. 40 (2005) 1289–1292.
[38] M. Vehkamäki, T. Hatanpää, M. Ritala, M. Leskelä, S. Väyrynen, E. Rauhala, Atomic layer deposition of $BaTiO_3$ thin films—effect of barium hydroxide formation, Chem. Vap. Deposition 13 (2007) 239–246.
[39] J. Zeng, H. Wang, M. Wang, S. Shang, Z. Wang, C. Lin, Preparation and ferroelectric properties of $BaTiO_3$ thin films by atmospheric-pressure metalorganic chemical vapor deposition, Thin Solid Films 322 (1998) 104–107.
[40] K.M. Ring, K.L. Kavanagh, Substrate effects on the ferroelectric properties of fine-grained $BaTiO_3$ films, J. Appl. Phys. 94 (2003) 5982.
[41] L. Qiao, X. Bi, Microstructure and ferroelectric properties of $BaTiO_3$ films on $LaNiO_3$ buffer layers by rf sputtering, J. Cryst. Growth 310 (2008) 2780–2784.
[42] L. Qiao, X. Bi, Domain configuration and phase transition for $BaTiO_3$ thin films on tensile Si substrates, J. Cryst. Growth 310 (2008) 5327–5330.
[43] B. Li, W. Shang, Z. Hu, N. Zhang, Template-free fabrication of pure single-crystalline $BaTiO_3$ nano-wires by molten salt synthesis technique, Ceram. Int. 40 (2014) 73–80.
[44] V.a. Zhabrev, L.P. Efimenko, V.G. Baryshnikov, I.G. Polyakova, a.V. Gumennikov, Synthesis of $BaTiO_3$ powders of different dispersities by the exchange reactions in molten salts, Glass Phys. Chem. 34 (2011) 91–96.
[45] D. Lv, R. Zuo, S. Su, Processing and morphology of (111) $BaTiO_3$ crystal platelets by a two-step molten salt method, J. Am. Ceram. Soc. 95 (2012) 1838–1842.
[46] Y. Zhang, L. Wang, D. Xue, Molten salt route of well dispersive barium titanate nanoparticles, Powder Technol. 217 (2012) 629–633.
[47] N. Kumada, A. Miura, T. Takei, I.B. Adilina, S. Shimazu, Low temperature synthesis of $ATiO_3$ (A: Mg, Ca, Sr, Ba) by using molten salt, J. Ceram. Soc. Jpn. 121 (2013) 74–79.
[48] L.J. McGilly, a Schilling, J.M. Gregg, Domain bundle boundaries in single crystal $BaTiO_3$ lamellae: searching for naturally forming dipole flux-closure/quadrupole chains, Nano Lett. 10 (2010) 4200–4205.
[49] D. Hennings, S. Schreinemacher, H. Schreinemacher, Solid-state preparation of $BaTiO_3$ – based dielectrics, using ultrafine raw materials, J. Am. Ceram. Soc. 84 (2001) 2777–2782.
[50] C. Pithan, D. Hennings, R. Waser, Progress in the synthesis of nanocrystalline $BaTiO_3$ powders for MLCC, Int. J. Appl. Ceram. Technol. 2 (2005) 1–14.
[51] M.T. Buscaglia, M. Bassoli, V. Buscaglia, R. Alessio, Solid-state synthesis of ultrafine $BaTiO_3$ powders from nanocrystalline $BaCO_3$ and $TiO_2$, J. Am. Ceram. Soc. 88 (2005) 2374–2379.
[52] R. Yanagawa, M. Senna, C. Ando, H. Chazono, H. Kishi, Preparation of 200 nm $BaTiO_3$ particles with their tetragonality 1.010 via a solid-state reaction preceded by agglomeration-free mechanical activation, J. Am. Ceram. Soc. 90 (2007) 809–814.
[53] M.M. Vijatovic, J.D. Bobic, B.D. Stojanovic, History and challenges of barium titanate: Part I, Sci. Sinter. 40 (2008) 155–165.
[54] M.M. Vijatovic, J.D. Bobic, B.D. Stojanovic, History and challenges of barium titanate: Part II, Sci. Sinter. 40 (2008) 235–244.
[55] L.L. Hench, J.K. West, The sol-gel process, Chem. Rev. 90 (1990) 33–72.
[56] O.A. Harizanov, Sol–gel $BaTiO_3$ from a peptized solution, Mater. Lett. 34 (1998) 232–236.
[57] L. Wang, L. Liu, D. Xue, H. Kang, C. Liu, Wet routes of high purity $BaTiO_3$ nanopowders, J. Alloy. Compd. 440 (2007) 78–83.
[58] Z. Zhao, V. Buscaglia, M. Viviani, M. Buscaglia, L. Mitoseriu, A. Testino, et al., Grain-size effects on the ferroelectric behavior of dense nanocrystalline $BaTiO_3$ ceramics, Phys. Rev. B 70 (2004) 024107.
[59] K. Byrappa, M. Yoshimura, Handbook of Hydrothermal Technology, Noyes Publications, Norwich, New York, USA, n.d.
[60] W. Suchanek, M. Lencka, R. Riman, Hydrothermal synthesis of ceramic materials, in: D. Palmer, R. Fernandez-Prini, A. Harvey (Eds.), Aqueous Systems at Elevated Temperatures and Pressures: Physical Chemistry in Water, STeam and Hydrothermal Solutions, first ed., Elsevier Ltd., London, UK, 2004, pp. 717–744.
[61] R.I. Walton, F. Millange, R.I. Smith, T.C. Hansen, D. O'Hare, Real time observation of the hydrothermal crystallization of barium titanate using in situ neutron powder diffraction, J. Am. Chem. Soc. 123 (2001) 12547–12555.
[62] R.I. Walton, Subcritical solvothermal synthesis of condensed inorganic materials, Chem. Soc. Rev. 31 (2002) 230–238.
[63] M. Lin, Z.Y. Fu, H.R. Tan, J.P.Y. Tan, S.C. Ng, E. Teo, Hydrothermal synthesis of $CeO_2$ nanocrystals : Ostwald ripening or oriented attachment ?, Cryst Growth Des. 12 (2012) 3296–3303.
[64] M. Mohammadikish, Hydrothermal synthesis, characterization and optical properties of ellipsoid shape $\alpha$-$Fe_2O_3$ nanocrystals, Ceram. Int. 1, Part B, (2013) 1–8.
[65] Z. Shao, W. Zhou, Z. Zhu, Advanced synthesis of materials for intermediate-temperature solid oxide fuel cells, Prog. Mater Sci. 57 (2012) 804–874.
[66] R.M. Piticescu, R.R. Piticescu, D. Taloi, V. Badilita, Hydrothermal synthesis of ceramic nanomaterials for functional applications, Nanotechnology 14 (2003) 312–317.
[67] A. Habib, R. Haubner, N. Stelzer, Effect of temperature, time and particle size of Ti precursor on hydrothermal synthesis of barium titanate, Mater. Sci. Eng., B 152 (2008) 60–65.
[68] J. Ovenstone, K.C. Chan, C.B. Ponton, Hydrothermal processing and characterisation of doped lanthanum chromite for use in SOFCs, J. Mater. Sci. 37 (2002) 3315–3322.
[69] S. Sōmiya, R. Roy, Hydrothermal synthesis of fine oxide powders, Bull. Mater. Sci. 23 (2000) 453–460.
[70] K. Byrappa, T. Adschiri, Hydrothermal technology for nanotechnology, Prog. Cryst. Growth Charact. Mater. 53 (2007) 117–166.
[71] R. Asiaie, W. Zhu, S.A. Akbar, P.K. Dutta, Characterization of submicron particles of tetragonal, Chem. Mater. 8 (1996) 226–234.
[72] M.-S. Zhang, Z. Yin, Q. Chen, W. Zhang, W. Chen, Study of structural and photoluminescent properties in barium titanate nanocrystals synthesized by hydrothermal process, Solid State Commun. 119 (2001) 659–663.
[73] H. Xu, L. Gao, Tetragonal nanocrystalline barium titanate powder : preparation, characterization, and dielectric properties, J. Am. Ceram. Soc. 86 (2003) 203–205.
[74] L. Guo, H. Luo, J. Gao, L. Guo, J. Yang, Microwave hydrothermal synthesis of barium titanate powders, Mater. Lett. 60 (2006) 3011–3014.
[75] N. Nuraje, K. Su, a. Haboosheh, J. Samson, E.P. Manning, N. -l. Yang, et al., Room Temperature Synthesis of Ferroelectric Barium Titanate Nanoparticles Using Peptide Nanorings as Templates, Adv. Mater. 18 (2006) 807–811.
[76] X. Wu, Z. Chen, Z. Cui, Low temperature synthesis of cubic BaTiO3 nanoparticles, The 8th Annual IEEE International Conference on Nano/Micro Engineered and Molecular Systems 1 (2013) 399–402.
[77] A.R. Tao, K. Niesz, D.E. Morse, Bio-inspired nanofabrication of barium titanate, J. Mater. Chem. 20 (2010) 7916.
[78] S. O'Brien, L. Brus, C.B. Murray, Synthesis of monodisperse nanoparticles of barium titanate: toward a generalized strategy of oxide nanoparticle synthesis, J. Am. Chem. Soc. 123 (2001) 12085–12086.
[79] T. Adschiri, Y. Hakuta, K. Arai, Hydrothermal synthesis of metal oxide fine particles at supercritical conditions, Ind. Eng. Chem. Res. 39 (2000) 4901–4907.
[80] T. Adschiri, Y. Hakuta, K. Sue, K. Arai, Hydrothermal synthesis of metal oxide nanoparticles at supercritical conditions, J. Nanopart. Res. 3 (2001) 227–235.
[81] M. Atashfaraz, M. Shariatyniassar, S. Ohara, K. Minami, M. Umetsu, T. Naka, et al., Effect of titanium dioxide solubility on the formation of $BaTiO_3$ nanoparticles in supercritical water, Fluid Phase Equilib. 257 (2007) 233–237.
[82] C. Aymonier, A. Loppinet-Serani, H. Reverón, Y. Garrabos, F. Cansell, Review of supercritical fluids in inorganic materials science, J. Supercrit. Fluids 38 (2006) 242–251.
[83] J.F. Bocquet, K. Chhor, C. Pommier, Barium titanate powders synthesis from solvothermal reaction and supercritical treatment, Mater. Chem. Phys. 57 (1999) 273–280.
[84] B. Chevalier, A. Demourgues, J. Etourneau, C. Even, A. Tressaud, Y. Garrabos, et al., Supercritical fluid processing: a new route for materials synthesis, J. Mater. Chem. 9 (1999) 67–75.
[85] Y. Hakuta, H. Ura, H. Hayashi, K. Arai, Effect of water density on polymorph of $BaTiO_3$ nanoparticles synthesized under sub and supercritical water conditions, Mater. Lett. 59 (2005) 1387–1390.
[86] Y. Hakuta, H. Hayashi, K. Arai, Fine particle formation using supercritical fluids, Curr. Opin. Solid State Mater. Sci. 7 (2003) 341–351.
[87] Y. Hakuta, H. Ura, H. Hayashi, K. Arai, Continuous production of $BaTiO_3$ nanoparticles by hydrothermal synthesis, Ind. Eng. Chem. Res. 44 (2005) 840–846.
[88] H. Hayashi, Y. Hakuta, Hydrothermal synthesis of metal oxide nanoparticles in supercritical water, Materials 3 (2010) 3794–3817.
[89] H. Hayashi, T. Noguchi, N.M. Islam, Y. Hakuta, Y. Imai, N. Ueno, Hydrothermal synthesis of $BaTiO_3$ nanoparticles using a supercritical continuous flow reaction system, J. Cryst. Growth 312 (2010) 1968–1972.
[90] K. Matsui, T. Noguchi, N. Islam, Y. Hakuta, H. Hayashi, Rapid synthesis of $BaTiO_3$ nanoparticles in supercritical water by continuous hydrothermal flow reaction system, J. Cryst. Growth 310 (2008) 2584–2589.
[91] H. Reverón, C. Aymonier, A. Loppinet-Serani, C. Elissalde, M. Maglione, F. Cansell, Single-step synthesis of well-crystallized and pure barium titanate nanoparticles in supercritical fluids, Nanotechnology 16 (2005) 1137–1143.
[92] R. Sui, P. Charpentier, Synthesis of metal oxide nanostructures by direct sol–gel chemistry in supercritical fluids, J. Chem. Rev. 112 (2012) 3057–3082.
[93] C. Gomez-Yanez, C. Benitez, H. Balmori-Ramirez, Mechanical activation of the synthesis reaction of BaTiO3 from a mixture of $BaCO_3$ and $TiO_2$ powders, Ceram. Int. 26 (2000) 271–277.
[94] V. Berbenni, A. Marini, G. Bruni, Effect of mechanical milling on solid state formation of $BaTiO_3$ from $BaCO_3 \pm TiO_2$ (rutile) mixtures, Thermochim. Acta 374 (2001) 151–158.
[95] L. Kong, J. Ma, H. Huang, R. Zhang, W. Que, Barium titanate derived from mechanochemically activated powders, J. Alloy. Compd. 337 (2002) 226–230.

[96] E. Brzozowski, M.S. Castro, Lowering the synthesis temperature of high-purity $BaTiO_3$ powders by modifications in the processing conditions, Thermochim. Acta 398 (2003) 123–129.
[97] M.T. Buscaglia, M. Bassoli, V. Buscaglia, R. Vormberg, Solid-state synthesis of nanocrystalline $BaTiO_3$: reaction kinetics and powder properties, J. Am. Ceram. Soc. 91 (2008) 2862–2869.
[98] M.T. Buscaglia, V. Buscaglia, R. Alessio, Coating of $BaCO_3$ crystals with $TiO_2$: versatile approach to the synthesis of $BaTiO_3$ tetragonal nanoparticles, Chem. Mater. 19 (2007) 711–718.
[99] F. Cansell, C. Aymonier, A. Loppinet-Serani, Review on materials science and supercritical fluids, Curr. Opin. Solid State Mater. Sci. 7 (2003) 331–340.
[100] E. Reverchon, R. Adami, Nanomaterials and supercritical fluids, J. Supercrit. Fluids 37 (2006) 1–22.
[101] F. Cansell, C. Aymonier, Design of functional nanostructured materials using supercritical fluids, J. Supercrit. Fluids 47 (2009) 508–516.
[102] C. Morin, A. Loppinet-Serani, F. Cansell, C. Aymonier, Near- and supercritical solvolysis of carbon fibre reinforced polymers (CFRPs) for recycling carbon fibers as a valuable resource: state of the art, J. Supercrit. Fluids 66 (2012) 232–240.
[103] A. Loppinet-Serani, C. Aymonier, F. Cansell, Supercritical water for environmental technologies, J. Chem. Technol. Biotechnol. 85 (2010) 583–589.
[104] A. Laaksonen, P.G. Kusalik, I.M. Svishchev, Three-dimensional structure in water–methanol mixtures, J. Phys. Chem. A 101 (1997) 5910–5918.
[105] A.R. Bazaev, I.M. Abdulagatov, E.A. Bazaev, A. Abdurashidova, (p, v, T, x) Measurements of $(1-x)H_2O + xC_2H_5OH$ mixtures in the near-critical and supercritical regions, J. Chem. Thermodyn. 39 (2007) 385–411.
[106] W.L. Marshall, E. V Jones, Liquid-vapor critical temperatures of several aqueous-organic and organic-organic solution systems, J. Inorg. Nucl. Chem. 36 (1974) 2319–2323.
[107] J. Griswold, J.D. Haney, V.A. Klein, Ethanol–water system: vapor–liquid properties at high pressures, Ind. Eng. Chem. 35 (1943) 701–704.
[108] F. Barr-David, B. Dodge, Vapor–liquid equilibrium at high pressures: the systems ethanol–water and 2-propanol–water, J. Chem. Eng. Data 4 (1959) 107–121.
[109] T. Adschiri, K. Kanazawa, K. Arai, Crystalization of Metal Oxide Particle through Hydrolysis in Supercritical Water, in: World Congress of Chemical Engineering, 1991.
[110] C. Slostowski, S. Marre, O. Babot, T. Toupance, C. Aymonier, Near- and supercritical alcohols as solvents and surface modifiers for the continuous synthesis of cerium oxide nanoparticles, Langmuir: ACS J. Surf. Colloids 28 (2012) 16656–16663.
[111] Y. Hakuta, S. Onai, H. Terayama, T. Adschiri, K. Arai, Production of ultra-fine ceria particles by hydrothermal synthesis under supercritical conditions, J. Mater. Sci. Lett. 17 (1998) 1211–1213.
[112] H. Hayashi, T. Noguchi, N.M. Islam, Y. Hakuta, Y. Imai, N. Ueno, Hydrothermal synthesis of organic hybrid $BaTiO_3$ nanoparticles using a supercritical continuous flow reaction system, J. Cryst. Growth 312 (2010) 3613–3618.
[113] J. Lu, K. Minami, S. Takami, T. Adschiri, Rapid and continuous synthesis of cobalt aluminate nanoparticles under subcritical hydrothermal conditions with in-situ surface modification, Chem. Eng. Sci. 85 (2013) 50–54.
[114] T. Adschiri, K. Kanazawa, K. Arai, Rapid and continuous hydrothermal crystallization of metal oxide particles in supercritical water, J. Am. Ceram. Soc. 75 (1992) 1019–1022.
[115] T. Adschiri, K. Kanazawa, K. Arai, Rapid and continuous hydrothermal synthesis of boehmite particles in subcritical and supercritical water, ChemInform 75 (1992) 2615–2618.
[116] Y. Hakuta, K. Seino, H. Ura, T. Adschiri, H. Takizawa, K. Arai, Production of phosphor (YAG: Tb) fine particles by hydrothermal synthesis in supercritical water, J. Mater. Chem. 9 (1999) 2671–2674.
[117] J.D. Holmes, K.J. Ziegler, R.C. Doty, L.E. Pell, K.P. Johnston, B.a. Korgel, Highly luminescent silicon nanocrystals with discrete optical transitions, J. Am. Chem. Soc. 123 (2001) 3743–3748.
[118] S. Desmoulins-Krawiec, C. Aymonier, F. Weill, S. Grosse, J. Etourneau, F. Cansell, et al., Synthesis of nanostructured materials in supercritical ammonia: nitrides, metals and oxides, J. Mater. Chem. 14 (2004) 228.
[119] J.J. Watkins, J.M. Blackburn, T.J. McCarthy, Chemical fluid deposition: reactive deposition of platinum metal from carbon dioxide solution, Chem. Mater. 11 (1999) 213–215.
[120] P.S. Shah, J.D. Holmes, R.C. Doty, K.P. Johnston, B.A. Korgel, Steric stabilization of nanocrystals in supercritical $CO_2$ using fluorinated ligands, J. Am. Chem. Soc. 122 (2000) 4245–4246.
[121] P.S. Shah, S. Husain, K.P. Johnston, B.A. Korgel, Nanocrystal arrested precipitation in supercritical carbon dioxide, J. Phys. Chem. B 105 (2001) 9433–9440.
[122] P.S. Shah, S. Husain, K.P. Johnston, B.A. Korgel, Role of steric stabilization on the arrested growth of silver nanocrystals in supercritical carbon dioxide, J. Phys. Chem. B 106 (2002) 12178–12185.
[123] A. Kameo, T. Yoshimura, K. Esumi, Preparation of noble metal nanoparticles in supercritical carbon dioxide, Colloids Surf., A 215 (2003) 181–189.
[124] M.C. McLeod, W.F. Gale, C.B. Roberts, Metallic nanoparticle production utilizing a supercritical carbon dioxide flow process, Langmuir: ACS J. Surf. Colloids 20 (2004) 7078–7082.
[125] H. Reverón, C. Elissalde, C. Aymonier, C. Bousquet, M. Maglione, F. Cansell, Continuous supercritical synthesis and dielectric behaviour of the whole BST solid solution, Nanotechnology 17 (2006) 3527–3532.
[126] H. Reverón, C. Elissalde, C. Aymonier, O. Bidault, M. Maglione, F. Cansell, Supercritical fluid route for synthesizing crystalline barium strontium titanate nanoparticles, J. Nanosci. Nanotechnol. 5 (2005) 1741–1744.
[127] E.S. Ilin, S. Marre, V. Jubera, C. Aymonier, Continuous supercritical synthesis of high quality UV-emitting ZnO nanocrystals for optochemical applications, J. Mater. Chem. C 1 (2013) 5058.
[128] A.I. Cooper, Recent developments in materials synthesis and processing using supercritical $CO_2$, Adv. Mater. 13 (2001) 1111–1114.
[129] T. Gendrineau, S. Marre, M. Vaultier, M. Pucheault, C. Aymonier, Microfluidic synthesis of palladium nanocrystals assisted by supercritical $CO_2$: tailored surface properties for applications in boron chemistry, Angewandte Chemie (International Ed. in English) 51 (2012) 8525–8528.
[130] K.S. Morley, P.C. Marr, P.B. Webb, A.R. Berry, F.J. Allison, G. Moldovan, et al., Clean preparation of nanoparticulate metals in porous supports: a supercritical route, J. Mater. Chem. 12 (2002) 1898–1905.
[131] V. Pessey, R. Garriga, F. Weill, B. Chevalier, J. Etourneau, F. Cansell, Control of particle growth by chemical transformation in supercritical $CO_2$/ethanol mixtures, J. Mater. Chem. 12 (2002) 958–965.
[132] E. Reverchon, G. Caputo, S. Correra, P. Cesti, Synthesis of titanium hydroxide nanoparticles in supercritical carbon dioxide on the pilot scale, J. Supercrit. Fluids 26 (2003) 253–261.
[133] W.E. Stallings, H.H. Lamb, N. Carolina, Synthesis of nanostructured titania powders via hydrolysis of titanium isopropoxide in supercritical carbon dioxide, Langmuir 19 (2003) 2989–2994.
[134] R. Garriga, V. Pessey, F. Weill, B. Chevalier, J. Etourneau, F. Cansell, Kinetic study of chemical transformation in supercritical media of bis(hexafluoroacetylacetonate)copper (II) hydrate, J. Supercrit. Fluids 20 (2001) 55–63.
[135] E. Grigorova, F. Cansell, B. Chevalier, A ddition of nanosized $Cr_2O_3$ to magnesium for improvement of the hydrogen sorption properties, J. Alloy. Compd. 351 (2003) 217–221.
[136] K. Sue, K. Murata, K. Kimura, K. Arai, Continuous synthesis of zinc oxide nanoparticles in supercritical water, Green Chem. 5 (2003) 659.
[137] A. Cabañas, M. Poliakoff, The continuous hydrothermal synthesis of nano-particulate ferrites in near critical and supercritical water, J. Mater. Chem. 11 (2001) 1408–1416.
[138] G. Philippot, K.M.Ø. Jensen, M. Christensen, C. Elissalde, M. Maglione, B.B. Iversen, et al., Coupling in situ synchrotron radiation with ex situ spectroscopy characterizations to study the formation of $Ba_{1-x}Sr_xTiO_3$ nanoparticles in supercritical fluids, J. Supercrit. Fluids 87 (2014) 111–117.
[139] Y. Roig, S. Marre, T. Cardinal, C. Aymonier, Synthesis of exciton luminescent ZnO nanocrystals using continuous supercritical microfluidics, Angewandte Chemie (International Ed. in English) 50 (2011) 12071–12074.
[140] E. Taboada, R. Solanas, E. Rodríguez, R. Weissleder, A. Roig, Supercritical-fluid-assisted one-pot synthesis of biocompatible core($\gamma$-$Fe_2O_3$)/shell($SiO_2$) nanoparticles as high relaxivity $T_2$-contrast agents for magnetic resonance imaging, Adv. Funct. Mater. 19 (2009) 2319–2324.
[141] C. Aymonier, C. Elissalde, H. Reveron, F. Weill, M. Maglione, F. Cansell, Supercritical fluid technology of nanoparticle coating for new ceramic materials, J. Nanosci. Nanotechnol. 5 (2005) 980–983.
[142] L. Matějová, Z. Matěj, R. Fajgar, T. Cajthaml, O. Šolcová, $TiO_2$ powders synthesized by pressurized fluid extraction and supercritical drying: effect of water and methanol on structural properties and purity, Mater. Res. Bull. 47 (2012) 3573–3579.
[143] T. Adschiri, Y.-W. Lee, M. Goto, S. Takami, Green materials synthesis with supercritical water, Green Chem. 13 (2011) 1380–1390.
[144] C. Elissalde, H. Reverón, C. Aymonier, D. Michau, F. Cansell, M. Maglione, The ferroelectric transition temperature as an intrinsic probe for sintered nanocrystalline $BaTiO_3$ synthesized under supercritical conditions, Nanotechnology 16 (2005) 797–802.
[145] H. Salehi, M. Hosseini, N. Shahtahmasebi, First-principles study of the electronic structure of $BaTiO_3$ using different approximations, Chin. J. Phys. 42 (2004) 619–628.
[146] X.Y. Xue, C.L. Wang, W.L. Zhong, The atomic and electronic structure of the $TiO_2$- and BaO-terminated $BaTiO_3$(0 0 1) surfaces in a paraelectric phase, Surf. Sci. 550 (2004) 73–80.
[147] S. Qin, D. Liu, H. Liu, Z. Zuo, Size-dependent selective etching mechanism: cavity formation on barium titanate nanocubes, J. Phys. Chem. C 112 (2008) 17171–17174.
[148] G.-Z. Wang, C.-R. Li, J. Cui, Z.-Y. Man, Ab initio study of $ATiO_3$ (0 0 1) surfaces, Surf. Interface Anal. 41 (2009) 918–923.
[149] V. Buscaglia, M.T. Buscaglia, M. Viviani, L. Mitoseriu, P. Nanni, V. Trefiletti, et al., Grain size and grain boundary-related effects on the properties of nanocrystalline barium titanate ceramics, J. Eur. Ceram. Soc. 26 (2006) 2889–2898.
[150] W.-S. Cho, Structural evolution and caracterization of $BaTiO_3$ nanoparticles synthesized from polymeric precursor, J. Phys. Chem. Solid 59 (1998) 659–666.
[151] I.J. Clark, T. Takeuchi, N. Ohtoric, D.C. Sinclaira, Hydrothermal synthesis and characterisation of $BaTiO_3$ fine powders: precursors, polymorphism and properties, J. Mater. Chem. 9 (1999) 83–91.
[152] E. Chávez, S. Fuentes, R.a. Zarate, L. Padilla-Campos, Structural analysis of nanocrystalline $BaTiO_3$, J. Mol. Struct. 984 (2010) 131–136.
[153] S.W. Lu, B.I. Lee, Z.L. Wang, W.D. Samuels, Hydrothermal synthesis and structural characterization of $BaTiO_3$ nanocrystals, J. Cryst. Growth 219 (2000) 269–276.

[154] B. Lee, J. Zhang, Preparation, structure evolution and dielectric properties of $BaTiO_3$ thin films and powders by an aqueous sol–gel process, Thin Solid Films 388 (2001) 107–113.
[155] T. Makino, M. Arimura, K. Fujiyoshi, Y. Yamashita, M. Kuwabara, Crystallinity of barium titanate nanoparticles synthesized by sol–gel method, Key Eng. Mater. 350 (2007) 31–34.
[156] S. Fuentes, E. Chávez, L. Padilla-Campos, D.E. Diaz-Droguett, Influence of reactant type on the Sr incorporation grade and structural characteristics of $Ba_{1-x}Sr_xTiO_3$ ($x = 0-1$) grown by sol–gel-hydrothermal synthesis, Ceram. Int. 39 (2013) 8823–8831.
[157] L. Qi, B.I. Lee, P. Badheka, L.-Q. Wang, P. Gilmour, W.D. Samuels, et al., Low-temperature paraelectric–ferroelectric phase transformation in hydrothermal $BaTiO_3$ particles, Mater. Lett. 59 (2005) 2794–2798.
[158] X. Zhu, J. Zhu, S. Zhou, Z. Liu, N. Ming, D. Hesse, $BaTiO_3$ nanocrystals: hydrothermal synthesis and structural characterization, J. Cryst. Growth 283 (2005) 553–562.
[159] R. Waser, Solubility of hydrogen defects in doped and undoped $BaTiO_3$, J. Am. Ceram. Soc. 71 (1988) 58–63.
[160] G. Busca, V. Buscaglia, M. Leoni, P. Nanni, Solid-state and surface spectroscopic characterization of $BaTiO_3$, Chem. Mater. 6 (1994) 955–961.
[161] E. Shi, C. Xia, W. Zhong, B. Wang, C. Feng, Crystallographic properties of hydrothermal barium titanate crystallites, J. Am. Ceram Soc. 80 (1997) 1567–1572.
[162] V. Petkov, M. Gateshki, M. Niederberger, Y. Ren, Atomic-scale structure of nanocrystalline $Ba_xSr_{1-x}TiO_3$ ($x = 1, 0.5, 0$) by X-ray diffraction and the atomic pair distribution function technique, Chem. Mater. 18 (2006) 814–821.
[163] C.J. Xiao, Z.H. Chi, W.W. Zhang, F.Y. Li, S.M. Feng, C.Q. Jin, et al., The phase transitions and ferroelectric behavior of dense nanocrystalline $BaTiO_3$ ceramics fabricated by pressure assisted sintering, J. Phys. Chem. Solids 68 (2007) 311–314.
[164] S. Wada, H. Yasuno, T. Hoshina, H. Kakemoto, Y. Kameshima, T. Tsurumi, Size dependence of THz region dielectric properties for barium titanate fine particles, J. Electroceram. 21 (2007) 198–201.
[165] X. Tian, J. Li, K. Chen, J. Han, S. Pan, Y. Wang, et al., Nearly monodisperse ferroelectric $BaTiO_3$ hollow nanoparticles: size-related solid evacuation in ostwald-ripening-induced hollowing process, Cryst. Growth Des. 10 (2010) 3990–3995.
[166] D.F.K. Hennings, C. Metzmacher, B.S. Schreinemacher, Defect chemistry and microstructure of hydrothermal barium titanate, J. Am. Ceram. Soc. 84 (2001) 179–182.
[167] W. Lu, M. Quilitz, H. Schmidt, Nanoscaled $BaTiO_3$ powders with a large surface area synthesized by precipitation from aqueous solutions: preparation, characterization and sintering, J. Eur. Ceram. Soc. 27 (2007) 3149–3159.